Editorial Manager(tm) for Zeitschrift für Metallkunde: International Journal of Materials Research
Manuscript Draft

Manuscript Number: MR1521R2

Title: Long Range Internal Stresses in Monotonically and Cyclically Deformed Metallic Single Crystals

Article Type: ISPMA-11 Structural Materials

Section/Category: Basic

Keywords: Long-range internal stress, Backstress, Synchrotron, Microdiffraction

Corresponding Author: Professor and Chair michael ernest kassner, Ph.D.

Corresponding Author's Institution: University of Southern California

First Author: michael ernest kassner, Ph.D.

Order of Authors: michael ernest kassner, Ph.D.; Peter geantil, MS; lyle e levine, PhD; Ben C Larson, PhD

Manuscript Region of Origin: UNITED STATES

Abstract: Selected experimental measurements and theoretical predictions for the magnitude of long-range internal stress (LRIS) in monotonically and cyclically deformed metals are assessed and recently developed, spatially-resolved x-ray microbeam techniques for direct measurements of LRIS are discussed. The results of previously reported differential-aperture x-ray microscopy (DAXM) spatially-resolved measurements of LRIS in dislocation cell interiors in monotonically deformed copper are compared with predictions and analyses associated with the composite model of deformation. In addition, the results of volume-integrating x-ray line-profile measurements and spatially-resolved DAXM measurements of strains in <100> oriented copper single crystals that were cyclically deformed to pre-saturation (without persistent slip bands) are presented.

Manuscript
Click here to download Manuscript: Prague_Paper_FINAL(1609).doc

# Long-range internal stresses in monotonically and cyclically deformed metallic single crystals

M.E. Kassner[a], P. Geantil[a], L.E. Levine[b], B. C. Larson[c]

[a]Aerospace and Mechanical Engineering, University of Southern California, Los Angeles, CA, USA
[b]Mater. Sci. and Eng. Lab., NIST, Gaithersburg, MD, USA
[c]Mater. Sci. Tech. Div., ORNL, Oak Ridge, TN, USA

Selected experimental measurements and theoretical predictions for the magnitude of long-range internal stress in monotonically and cyclically deformed metals are assessed and recently developed, spatially-resolved X-ray microbeam techniques for direct measurements of long-range internal stress are discussed. The results of previously reported differential-aperture X-ray microscopy spatially-resolved measurements of long-range internal stress in dislocation-cell interiors in monotonically deformed copper are compared with predictions and analyses associated with the composite model of deformation. In addition, the results of volume-integrating X-ray line-profile measurements and spatially-resolved differential-aperture X-ray microscopy measurements of strains in <100> oriented copper single crystals that were cyclically deformed to pre-saturation (without persistent slip bands) are presented.

**Keywords:** Long-range internal stress; Backstress; Synchrotron; Microdiffraction

## 1. Introduction

Plastic flow in ductile materials represents a longstanding issue of both fundamental and technological importance. Nevertheless, more than 75 years after the identification of dislocations as the source and more than 50 years after the first direct observation of single and aggregated dislocations by electron microscopy, our understanding of plasticity remains inadequate. It has been recognized that short- and long-range internal stresses (LRIS) play decisive roles in the generation and aggregation of dislocations on mesoscopic length scales [see e.g. 1,2]. However, the origin and precise role of LRIS has been the source of substantial debate as it relates to anelasticity, the Bauschinger effect, and cyclic deformation, as well as a fundamental understanding of plastic deformation in general.

### 1.1 Experimental evidence and predictions for long-range internal stresses in deformed metals

In this section, we provide a historical perspective of selected conventional experimental investigations probing LRIS in monotonically and/or cyclically deformed pure metals – mostly Cu, Al, and Ni. LRIS in deformed metals was first discussed in connection with the Bauschinger effect [1,3], where the material strain-hardens with increasing deformation loading, and on reversal of the direction of the loading, the flow stress is found to be less than for flow in the forward direction, just prior to reversal.

#### 1.1.1 The Bauschinger effect

The Bauschinger effect is important as it appears to be the basis for low hardening rates and low saturation stresses in fatigued materials. Pedersen [4] and Mughrabi [3] independently advanced the concept of elevated stresses in association with heterogeneous dislocation substructures (e.g., cell/subgrain walls, persistent slip band (PSB) walls, etc.). “Hard” regions (high dislocation density walls, etc.) and “soft” regions (low dislocation density channels, or cell interiors) are compatibly sheared. With the assumption that the hard and soft components yield at different stresses, it was suggested that the “composite” is under a heterogeneous stress state with the high-dislocation-density regions having the higher magnitude stress. Such a composite model may provide a rationalization for the Bauschinger effect; as soft and hard regions are unloaded from a tensile stress, the hard region eventually places the soft region in compression while the hard region is still under positive stress. Thus, the Bauschinger effect of plasticity occurs on stress reversal in the form of a lower average stress magnitude than just prior to unloading due to “reverse” plasticity in the soft region. The “composite” model for backstress (or LRIS) is illustrated in Fig. 1, where the LRIS are defined by

$$\tau_{\mathrm{w}}^{\mathrm{y}} = \tau_{\mathrm{a}} + \Delta\tau_{\mathrm{w}} \quad (1)$$

$$\tau_{\mathrm{I}}^{\mathrm{y}} = \tau_{\mathrm{a}} + \Delta\tau_{\mathrm{I}} \quad (2)$$

in which $\tau_{\mathrm{a}}$ is the applied stress, $\Delta\tau_{\mathrm{w}}$ and $\Delta\tau_{\mathrm{I}}$ are LRIS, and $\tau_{\mathrm{w}}^{\mathrm{y}}$ and $\tau_{\mathrm{I}}^{\mathrm{y}}$ are the local stresses in the walls and interiors, respectively, of the composite structure. That is, LRIS appear as local deviations from the applied stress in a loaded material. The basis for LRIS in single-phase systems is within the dislocation arrangements, themselves. With the disparity in yield stress between the high and low dislocation density regions leading to dislocation accumulation at the interface for compatibility. These are geometrically necessary dislocations (GNDs). It appears that LRIS can arise from a summation of the stress fields of individual GNDs [5]. The Bauschinger effect may actually involve *both* LRIS and an Orowan—Sleeswyk component that considers relatively large (reverse) strains that are not associated with LRIS [6,7].

Figure 1

### 1.1.2 X-ray line profile measurements

Indirect evidence for internal stresses has been based on X-ray diffraction (XRD) experiments generally subsequent to, but also during plastic deformation [2,3,8—13]. These experiments infer average *local* stresses based on spatially integrated diffraction from a very large number of cells. Basically, X-ray peaks have been observed to broaden asymmetrically with plasticity and the line profiles become increasingly asymmetric with increasing strain, although a pronounced asymmetry is not always observed (e.g., pure Al and materials cyclically deformed to pre-saturation, although recent work on Al appears to have observed asymmetry [14]). An additional general feature in such measurements is that the asymmetry reverses sign when changing from tension to compression deformation. Some investigators [10,11,15] unloaded their samples from various points in the hysteresis loop of single crystal Ni, and polycrystalline Cu, and these diffraction results were also consistent with the pattern of asymmetry reversal. Diffraction line-profile asymmetries have also been observed for cyclic deformation of Ni to saturation, for which persistent slip bands (PSB) were present; diffraction-peak asymmetry was not observed for pre-saturation cyclic deformation (i.e. no PSBs). From this result, it was concluded by Hecker et al. [10] and Bretschneider [16] that LRIS are present only when PSBs are present in cyclically deformed Ni.

Mughrabi et al. [3,2,12] modeled the asymmetric line profiles within the composite model by decomposing the diffraction peak into two symmetric peaks. One peak was interpreted as diffraction from the material in high-dislocation-density regions such as dipole bundles, persistent slip bands, cell walls, or subgrain boundaries with

high local stresses. The second peak was then interpreted as originating from the lower-dislocation-density regions presumed to originate from cell interiors where the stresses were predicted to be smaller in magnitude than the applied stress. Figure 2 illustrates the decomposition concept in which the characteristic asymmetric peak shape in a sample deformed in compression is associated with the sum of two symmetric peaks with weight ratios of 2.7:1 but offset slightly in angle (or scattering wavevector). Using such an analysis, for single crystal Cu compression deformation experiments, Ungar, et al. [17] suggested relatively low values of +0.10 $\sigma_A$ in the cell interiors and -0.4 $\sigma_A$ in the cell walls for a <100>-oriented Cu single crystal deformed to strains of roughly -0.30 (in compression). However, various investigators have reported stresses in the walls ranging from 1.4 to 2.8 times larger than the applied stress [8,10,18—21] the largest values were obtained for cyclic deformation for which PSBs were present. Theoretical work [22,23] has generally suggested LRIS values that exceed these experimental values.

Figure 2

Low-temperature neutron irradiation of cyclically deformed Cu under full stress was used by Mughrabi [3] to estimate the local stress between PSB dislocation walls. This study used TEM to study the (neutron-irradiation-pinned) dislocation loop radii as a function of position between the walls. The stresses were originally suggested to be roughly a factor of three higher than the applied stress for dipole bundles in Cu PSB walls. That is, according to Eqs. 1 and 2, the LRIS corresponded to about twice the applied stress. In-situ TEM by Lepinoux and Kubin [24] on cyclically deformed Cu was consistent with the original Mughrabi findings. However, recent work by Mughrabi et al. has suggested that the actual LRIS values may be half the earlier estimates [25].

### 1.1.3 Dipole height measurements

Electron microscopy measurements of dipole heights were performed on aluminum and copper single crystals (oriented for single slip) by Kassner et al. [26]. The average separation of dipoles is constant throughout the microstructure in cyclically deformed Cu, Ni, and Al, which could be interpreted as suggesting a uniform state of stress. The maximum dipole heights are the widest stable dipoles and suggest a maximum stress in the vicinity of the dipoles. The maximum dipole height translates to a stress that is about equal to the applied (cyclic) stress for Al. Hence, this is evidence of an absence of long-range internal stress in AL single crystals cyclically deformed to presaturation at LN (no PSBs). The stress to separate the widest dipoles is, however, only within a factor of 2—3 of the applied stress in Cu and a factor of four for that in Ni [26—29]. Overall, these results are ambiguous in terms of an assessment of LRIS.

### 1.1.4 Convergent beam electron diffraction

Convergent beam electron diffraction (CBED) experiments were also used to measure changes in the lattice parameter (internal stresses) in monotonically and cyclically deformed Cu and Al after unloading and thin sectioning [29,30]. CBED lattice parameter measurements were made by Kassner et al. with 20—100 nm beam sizes for two cases. The first was near (within 80 nm) dipole bundles and within the channels in Cu cyclically deformed to pre-saturation [29]; the second was near cell/subgrain walls and subgrain interiors in creep-deformed Al and Cu [30]. Although the experimental uncertainties were equal to the flow stress in cyclically deformed Cu and were 1.5 to 2 times the applied stress for creep tests, these measurements ruled out the presence of large LRIS (> 3x applied stress) such as reported experimentally [31] or predicted theoretically [18,22,23]. Of course, the thickness of the region of the foils examined in CBED was below 100 nm so that relaxation of LRIS could have occurred.

### 1.1.5 Mechanical estimates

Estimates of long-range internal stresses have been made, particularly at elevated temperature using the Gibbs stress-dip tests, by several investigators. These analyses are summarized in a recent book [32] and in [5]. Essentially, stress dip experiments, that are often coupled with theoretical modeling, have generally implied stresses in subgrain/cell walls that are on the order of 5—10 times the applied stress.

## 2. X-Ray microbeams as direct probes of long range internal stress

In this section we provide a more detailed description of a recently developed 3D X-ray microscopy technique for performing direct, spatially-resolved measurements of LRIS and describe in the following section its application for direct measurements of LRIS in dislocation cell interiors in single-crystalline Cu samples deformed in compression and tension. Exploiting the ultra-high brilliance of synchrotron X-ray radiation, the development of 3D X-ray microscopy with submicron 3D spatial resolution [33] has made it possible to probe the local crystal structure, orientation, and of particular interest here, elastic strain in single crystals, polycrystals, and deformed materials. As illustrated schematically in Fig. 3a, this technique makes use of polychromatic synchrotron X-rays focused (achromatically) to microbeam sizes ~0.5 μm diameter through the use of elliptically figured Kirkpatrick—Baez focusing mirrors. To obtain depth resolution along the half-micron-diameter beam, the technique uses differential-aperture (i.e. knife-edge) depth profiling of the diffracted x-rays by step-scanning a 50 μm Pt wire through the diffracted X-rays and collecting CCD images at each step [33]. CCD difference images between successive steps of the profiler provide a pinhole-camera-like image of all diffracted rays that pass through the submicron step-distance aperture; thus the name differential-aperture X-ray microscopy (DAXM). By translating the sample laterally in submicron steps and performing white-beam depth-profiling scans at each sample position, full 3D volumes can be imaged from the standpoint of local crystal orientations.

An analogous monochromatic DAXM scanning technique demonstrated by Yang et al. [34] utilizes the removeable/insertable monochromator shown in Fig. 3a that makes it possible to step-scan the energy of the X-ray microbeam to determine the energy of local Bragg reflections for each step of the depth profiling Pt wire. That is, nested energy and depth scanning makes it possible to determine the Bragg peak energy for each depth increment. Because the scattering angle for each pixel of the CCD detector is known from the calibration, it is possible to determine absolute lattice spacing (and hence elastic strains) with submicron spatial resolution in 3D and a strain accuracy of $+/-10^{-4}$ (one standard deviation). In essence, the depth-resolved strain measurement process is a straightforward application of Bragg's law in connection with geometrical knife-edge depth profiling that provides a direct and absolute capability to measure long-range internal stresses as a function of position along the X-ray microbeam. These capabilities have been implemented on Sector 34 of the Advanced Photon Source (APS) and their application has been discussed in detail elsewhere [33—37].

Figure 3

Because the Bragg energies change significantly with the crystal plane orientation, the Bragg energies across the entire white-beam Laue diffraction image in Fig. 3b corresponded to a range of ~ 600 eV. For measurements of dislocation-cell interior strains it is possible to locate the positions of individual sharp diffraction spots in the CCD pattern by manually scanning the energy of the monochromator across the ~600 eV range, selecting a sharp peak to study, and returning the monochromator to the corresponding energy. With the energy set, the center of the dislocation cell can be determined by moving the profiling wire across the diffracted beams until the desired peak intensity is half occluded. Dislocation cell lattice strain measurements can then be performed by a nested scan of the energy and depth over +/- 10 eV and +/-5 μm ranges, respectively, to determine the Bragg energy and the Bragg angle pertaining to the sharp Laue spots on the image. Combinations of relatively rapid manual scans just described and more time intensive fully automated nested energy and profiler scans were used to collect the dislocation-cell interior strain measurements reported in references [37] and [38].

## 3. X-ray microbeam measurements of LRIS in dislocation cell interiors in tension and compression-deformed copper

Figure 4 is a representative TEM micrograph made on a <001>-oriented single crystal Cu sample deformed in compression to a true strain of 28 % at room temperature showing a well-developed dislocation cell structure. It is clear that many, but not all, of the dislocation cells have sizes larger than the 0.5 μm diameter X-ray

microbeams; there exist regions in which the dislocation cells are either smaller than the 0.5 μm spatial resolution or they are cell structures not fully clean of dislocations. Accordingly, the 0.5 μm DAXM measurements can be expected to yield sharp diffraction peaks from the larger cells, while other regions can be expected to produce both diffuse-like diffraction features as well as relatively sharp peaks when the measured volume includes both dislocation-rich cell-wall regions and from the cell interior contributions. Indeed, such a combination of sharp spots and more diffuse scattering is observed in the Laue diffraction image on the detector in Fig. 3b, and accordingly, DAXM strain measurements were performed on the sharpest peaks (of both higher and lower intensity) and are associated with LRIS in well-developed dislocation cells in Fig. 5.

Figure 4

Figures 5 (a) and (b) show a superposition of conventional (i.e. spatially-integrated) (006) X-ray diffraction line profiles and individual (i.e. spatially-resolved) lattice strain measurements for both the compression (-0.277) and tension (+0.306) deformed Cu single-crystals [37]. We note that the cell interior strains, $\Delta d/d_o$, (and hence, stress) in the tensile-strained sample are negative (i.e. contracted) and the cell interior strains are positive (i.e. expanded) for the compression-deformed sample. We further note that this strain sign reversal follows the well-known reversal in the asymmetry [2,3,12] in the spatially integrated line profile measurements for compression- and tension-deformed samples. The spatially resolved results in Fig. 5 [37] represented the first direct measurements of LRIS in monotonically deformed Cu, where it was noted that the results for both compression and tension are in general agreement with the composite model predictions of Mughrabi [2].

Although the overall average elastic strains are in agreement with the composite model, the individual cell interior LRIS for tension and compression vary considerably from cell to cell over a rather wide range. As a fraction of the applied stress, the compression specimen stresses ranged from -0.03 to -0.51 and those from the tensile specimen ranged from -0.07 to 0.37, where the one-standard-deviation uncertainties in these measurements were ± 0.04. Twelve cell interiors were measured from the compression sample and nine from the tension specimen, so the statistical sampling was not large enough to extract reliable stress distribution functions.

Figure 5

In a follow-on microbeam study to increase statistical precision [38], 52 cell interior elastic strains were measured from a separate compression sample deformed to a true strain of 0.28 and a true stress of 210 MPa. This latter study provided a statistically robust sampling of the cell interior elastic strains within a total explored sample volume of 39 $\mu m^3$, giving an average LRIS of -0.17 ± 0.01 of the applied stress with, again, a relatively

wide range of strains comparable to the earlier [37] microbeam work.

All of the microbeam studies were conducted on unloaded specimens. Straub et al made in situ (under load) volume-averaged asymmetry measurements [39], in which the published X-ray diffraction line profiles exhibited the expected asymmetry under load at elevated temperature. Importantly, the *unloaded* specimen retained a majority of the asymmetry despite elevated-temperature exposure. If the asymmetry under load is indicative of LRIS, then unloading these specimens substantially "locks in" these stresses, confirming that the microbeam results reflect the distribution of stresses present under load.

## 4. X-Ray microbeam measurements of LRIS in cyclically deformed copper

We have performed LRIS measurements on copper single crystals oriented for single slip (i.e. near a <123> orientation) that were cyclically deformed to pre-saturation (no PSBs). Figure 6 shows a TEM micrograph indicating the pre-saturation cyclic deformation vein microstructure and it shows the final cycle of the 200 total cycle treatment. A strain amplitude of $1.25 \times 10^{-3}$ was used, which corresponds to a cumulative strain of about 1.0, or the sum of the absolute values of the strains imposed on the crystal. The samples, testing apparatus, and data acquisition are described in [29].

In Fig. 7 we present X-ray line-profile measurements (made using the 024 Bragg reflection) for the cyclically deformed Cu sample and for a low-dislocation undeformed Cu crystal. We note first of all that the line profile for the cyclically deformed Cu has a characteristic asymmetry similar to those in Fig. 5, and that the line profile for undeformed Cu is completely symmetric, indicating that the asymmetry is deformation-induced and not instrumental anisotropy. We note further that the line profile for the cyclically deformed sample is self-similar in shape, but nearly a factor of ten narrower than that for the tension-deformed sample in Fig. 5(b). Based on the cell-interior strain levels found for monotonic tensile and compression deformation in Fig. 5 that are ~5 x $10^{-4}$, and the fact that these values correspond approximately to the peaks of the asymmetric line profiles, the pre-saturation cyclic deformation results in Fig. 7 would suggest LRIS values in the range of ~0.5-1.0 x $10^{-4}$.

Figure 6

As with monotonically deformed specimens, depth-resolved microdiffraction experiments were performed on the cyclically deformed single crystals to measure the local strains directly. The specimen was scanned with the incident microbeam directed perpendicular to the dipole bundles in Fig. 6(b) (e.g. the [220] direction) in order to probe lattice parameters in both the high-dislocation-density veins (dipole bundles) and the low-dislocation-density channels. The scans revealed no changes in the lattice parameter to within the experimental

measurement uncertainties of $\pm 10^{-4}$. This uncertainty multiplied by the elastic modulus $E_{123}$ would correspond to a maximum stress $\cong E_{123} \times 10^{-4} = 13.1$ MPa or maximum LRIS values of about 0.34 of the applied stress. The dislocation densities in the dipole bundles and channels were $1.3 \times 10^{15}$ m$^{-2}$ and $8.3 \times 10^{12}$ m$^{-2}$ respectively (total dipole dislocation line-length per unit volume). Although it is unclear whether the line-profile asymmetry measured in Fig. 7 is indicative of LRIS or other effects such as dipole polarization (which can give rise to asymmetry independent of LRIS [40]), and of course higher-precision spatially resolved microbeam measurements are required to provide direct information on the spatial distribution of LRIS in these cyclically deformed samples. The presence of LRIS significantly larger than around one-third of the applied stress seems to be ruled out.

Figure 7

## 5. Discussion

There is reasonable agreement between our monotonic deformation results for Cu and the re-analyzed results of Mughrabi and Ungar et al. [12,27] for a <100>-oriented Cu single crystal deformed in tension to similar plastic strain. The estimates for the volume fractions of cell walls at -0.248 strain along [001] in <001>-oriented Cu in this work is $f_w \cong 0.44$—$0.58$, based on a fairly simple image analysis of TEM micrographs that separate "high"- and "low"-dislocation-density regions. This implies that if $\Delta\sigma_I \cong 0.17 - 0.28\ \sigma_A$, (where $\Delta\sigma_I$ is the normal stress counterpart to the shear LRIS in Eq. 2) then the average LRIS in the cell walls is expected to be about $0.17 - 0.56\ \sigma_A$ (and of opposite sign) if the values of $f_w$ by Mughrabi and Ungar [2] are also considered. The cell-wall estimates of LRIS are in rough agreement with the value of $0.4\ \sigma_A$ extracted by Mughrabi and Ungar based on X-ray diffraction-line profile measurements on unloaded Cu single crystal specimens, which represent an average over a very large number of cells. Our results as well as the Mughrabi and Ungar results are of course not in agreement with the larger values of LRIS anticipated by Blum et al. [8], Morris and Martin [31], Sedlacheck et al. [22], Gibleing and Nix [23], and Takeuchi and Argon [18].

Although the spatially resolved X-ray microbeam results reported here for pre-saturation level cyclic deformation in single-slip Cu represent only initial measurements for a specific cyclic deformation condition, they provide an upper bound of $\sim 10^{-4}$ for LRIS levels under these particular cyclic conditions. Moreover, considering the very small cyclic deformation broadening in Fig. 7 compared to Fig. 5, the (volume integrating) X-ray diffraction-line profile measurements presented are consistent with the very small LRIS implied by the spatially resolved strain measurements. Further spatially resolved LRIS measurements with higher precision are obviously needed for the pre-saturation regime (i.e. no PSBs) and spatially resolved microbeam

measurements of LRIS in deformation regimes that include PSBs will be required for comparisons with existing results such as those of Mughrabi et al. [25]

## 6. Summary

The results of measurements and predictions of the magnitudes of LRIS in monotonic and cyclically deformed metals over the last 25 years have varied widely – ranging up to more than ten times the applied stresses in some cases. However, more recent results and interpretations within the composite model have tended to project LRIS magnitudes less than or of the order of the applied stress. Direct spatially-resolved X-ray microbeam measurements of LRIS in dislocation cell interiors in monotonically deformed <100>-oriented copper single crystals have shown that LRIS in cell interiors vary significantly from cell to cell, but their average values vary from 0.16 to 0.29 times the applied stress. Initial spatially-resolved X-ray microbeam measurements of LRIS in <123> single-slip-oriented copper deformed cyclically to pre-saturation levels (so that PSBs were not present) indicated LRIS magnitudes to be at or below the present measurement uncertainties of +/- $10^{-4}$. However, X-ray line profile measurements indicate the presence of profile asymmetries self-similar, but much smaller in magnitude, to those observed for monotonically deformed copper.

**Acknowledgements**

MEK and PG acknowledge support from the Office of Basic Energy Sciences (BES), DOE. Research at ORNL is supported by DOE Office of Science, Basic Energy Sciences, Division of Materials Sciences & Engineering. The XOR/UNI facilities on Sectors 33 and 34 at APS are supported by USDOE, Office of Science.

**References**

[1] M. Zaiser, A. Seeger, in: [2], F.R. N. Nabarro, M. S. Duesbery (Eds.) Elsevier ch. 56 (2002) 3.

[2] H. Mughrabi, T. Ungar: Dislocations in Solids, Elsevier (2002) 345.

[3] H. Mughrabi: Acta Metall. 31 (1983) 1367—1379.

[4] O. B. Pedersen, L. M. Brown, W. M. Stobbs: Acta Metall. 29 (1981) 1843.

[5] M.E. Kassner, P. Geantil, L. E Levine, B.C. Larson: Mater. Sci. Forum, 604—609 (2009) 39—52.

[6] A.W. Sleeswyk, M.R. James, D.H. Plantinga, W.S.T. Maathius: Acta Metall. 26 (1978) 1265—1271.

[7] E. Orowan, in: G.M. Rassweiler, W.L. Grube (Eds.), Internal Stresses and Fatigue in Metals, General Motors Symposium, Amsterdam: Elsevier (1959) 59—80.

[8] A. Borbély, W. Blum, T. Ungar: Mater. Sci. Eng. 276 (2000) 186—194.

[9] A. Borbély, G. Hoffmann, E. Aernoudt, T. Ungar: Acta Mater. 45 (1997) 89—98.

[10] M. Hecker, E. Thiele, C. Holste: Mater. Sci. Eng. A234—236 (1997) 806—809.

[11] H. Biermann, T. Ungar, T. Pfannenmüller, G. Hoffmann, A. Borbély, H. Mughrabi: Acta. Metal. Mater. 41 (1993) 2743—2753.

[12] H. Mughrabi, T. Ungar, W. Kienle, M.Wilkens: Phil. Mag. A 53 (1986) 793—813.

[13] B. Jakobsen, H.F. Poulsen, U. Lienert, J. Almer, S.D. Shastri, H.O. Sørensen, C. Gundlach, W. Pantleon: Science 32 (2006) 889—892.

[14] W. Pantleon, H. Poulsen, J. Almer, U. Lienert: Mater. Sci Eng. 387—389A (2004) 339—342

[15] M. Hecker, E. Thiele, C. Holste: Z. Metall. 89 (1998) 203—210.

[16] Private communication with J. Bretschneider, Grenada, Spain, 1998.

[17] T. Ungar, H. Mughrabi, M. Wilkens, A. Hilscher: Phil. Mag. A 64 (1994) 495—496.

[18] A.S. Argon, S. Takeuchi: Acta Metall. 29 (1981) 1877.

[19] H. Mughrabi: Phil. Mag. A 86 (2006) 4037—4054.

[20] H. Mughrabi: Acta Mater. 54 (2006) 3417—3427.

[21] S. Straub, W. Blum, H.J. Maier, T. Ungar, A. Borbely, H. Renner: Acta Mater. 44 (1996) 4337—4350.

[22] R. Sedlacek , W. Blum, J. Kratochvil, S. Forest: Metall. Mater. Trans. 33A (2002) 319—327.

[23] J.C. Gibeling, W.D. Nix: Acta Metall. 28 (1980) 1743—1752.

[24] J. Lepinoux, L.P. Kubin: Phil. Mag. 57 (1985) 675—696.

[25] H. Mughrabi, F. Pschenitzka: Phil. Mag. 85 (2005) 3029—3045.

[26] M.E. Kassner, M.A. Wall: Metall. and Mater. Trans. 30A (1999) 777—779.

[27] B. Tippelt, J. Bretschneider, P. Hähner: Phys. Stat. Sol. A. 163 (1997) 11—26.

[28] J. Bretschneider, C. Holste, B. Tippelt: Acta Mater. 45 (1997) 3775—3783.

[29] M.E. Kassner, M.-T. Perez-Prado, K.S. Vecchio, M.A. Wall: Acta Mater. 48 (2000) 4247—4254. 381 (2001) 254—259.

[30] M.E. Kassner, M.T. Perez-Prado, M. Long, K.S. Vecchio: Metall. Mater. Trans. 33A (2002) 311—318.

[31] M.A. Morris, J.L. Martin: Acta Metall. 32 (1984) 1609—1623.

[32] M.E. Kassner, M.-T. Perez-Prado, Fundamentals of Creep in Metals and Alloys, Elsevier (2004) 1—217.

[33] B.C. Larson, W. Yang, G.E. Ice, J.D. Budai, J.S. Tischler: Nature 415 (2002) 887—890.

[34] W. Yang, B. C. Larson, G. E. Ice, J. Z. Tischler, J. D. Budai, K.-S. Chung, W. P. Lowe: Appl. Phys. Lett. 82(2003) 3856.

[35] G. Ice, B.C. Larson, W. Yang, J.D. Budai, J. Z. Tischler, J.W.L. Pang, R.I. Barabash, W. Liu: J. Synchrotron Radiat. 12 (2005) 155–162.

[36] W. Yang, B.C. Larson, J.Z. Tischler, G.E. Ice, J.D. Budai, W. Liu: Micron 35 (2004) 431—439

[37] L.E. Levine, B.C. Larson, W. Yang, M.E. Kassner, J.Z. Tischler, M.A. Delos-Reyes, R.J. Fields, W. Liu:[ Nature Materials 5 (2006) 619—622.

[38] L.E. Levine, B.C. Larson, M.E. Kassner, J. Tischler, P. Geantil: Zeitschr. Kristall., in press.

[39] S. Straub, W. Blum, H.J. Maier, T. Ungar, A. Borberly, H. Renner: Acta Mater. 44 (1996) 4337—4350.

[40] I. Gaal: Proc. 5th Int. Riso Symp., Riso National Lab (1984) 249—254.

Correspondence address:

Dr. Michael Kassner
University of Southern California
Department of Aerospace and Mechanical Engineering
Los Angeles, California 90089-1453
Tel.: (213) 740-7212
Fax: (213) 740-8071
e-mail: kassner@usc.edu

**Figure Captions**

Figure 1. The composite model illustrating the Bauschinger effect. The different stress versus strain behaviors of the (hard) cell walls and the (soft) cell interiors are illustrated in (a), while the stress versus strain behavior of the composite is illustrated in (b). When the composite is completely unloaded, the low-dislocation density cell interior region is under compressive (back) stress. This leads to a yielding of this "softer" component in compression at a "macroscopic" stress less than $-\tau_{avg}$.

Figure 2. Illustration of an asymmetric X-ray diffraction line profile from a compressed sample, generated by summing two symmetric sub-profiles (Gaussian peaks) with differing amplitudes, widths, and center positions. The narrow peak would come from the cell interiors and the smaller broad peak from the cell walls, as predicted by the Mughrabi composite model.

Figure 3. Submicron-resolution 3D X-ray microscopy using differential-aperture (i.e. knife-edge) depth profiling: (a) Schematic illustration of differential-aperture X-ray microscopy (DAXM) in which white X-rays are incident from the right; white or monochromatic X-rays are focused to a ~0.5 μm diameter microbeam with ~500 μm depth of field by achromatic Kirkpatrick-Baez focusing mirrors. White or monochromatic X-rays diffracted from the sample at varying depths are collected on the CCD X-ray detector while the profiling wire is stepped in submicron increments across the diffraction pattern; triangulation from each pixel position to the

profiler wire plus extrapolation back to the microbeam position determines the depth of the scattering site along the beam; (b) Illustration of the process of occluding individual diffraction peaks with the profiling wire that is used to determine the source depth along the microbeam and perform nested energy scans and profiler scans to determine dislocation cell interior strain.

Figure 4. The dislocation substructure of deformed [001]-oriented Cu single crystals compression deformed to a true strain of -0.28. The compression axis is perpendicular to the image and was taken under g=002 two-beam condition.

Figure 5. Spatially integrating (006) X-ray diffraction line profiles and spatially-resolved cell interior strains for (a) compression-deformed and (b) tension deformed <001>-oriented Cu single crystals. These results, reported in [37] and plotted as a function of lattice strain $\Delta d/d_o = -\Delta q/q$, show the measured line profiles, the reversal in asymmetry for compression and tension deformation (unloaded), and the measured strains (blue lines) for individual cell interiors, where $q = 4\pi \sin(\theta)/\lambda$ is the wavevector; $\theta$ is the scattering angle and $\lambda$ is the X-ray wavelength.

Figure 6. (a) Stress—strain profile for the last ($200^{th}$) cycle of the cyclic deformation. It's unknown whether the final cycle ended with a tensile or compressive stress; (b) TEM micrograph of the dislocation vein structure in a copper single crystal oriented for single slip and deformed cyclically at 298 K to about half of the saturation stress.

Figure 7. (a) Spatially integrated 024 X-ray diffraction line profiles measured on the fatigued copper single crystal and on a non-deformed copper reference sample. Note the large change in scale compared to Fig. 5.

**Line Drawing**

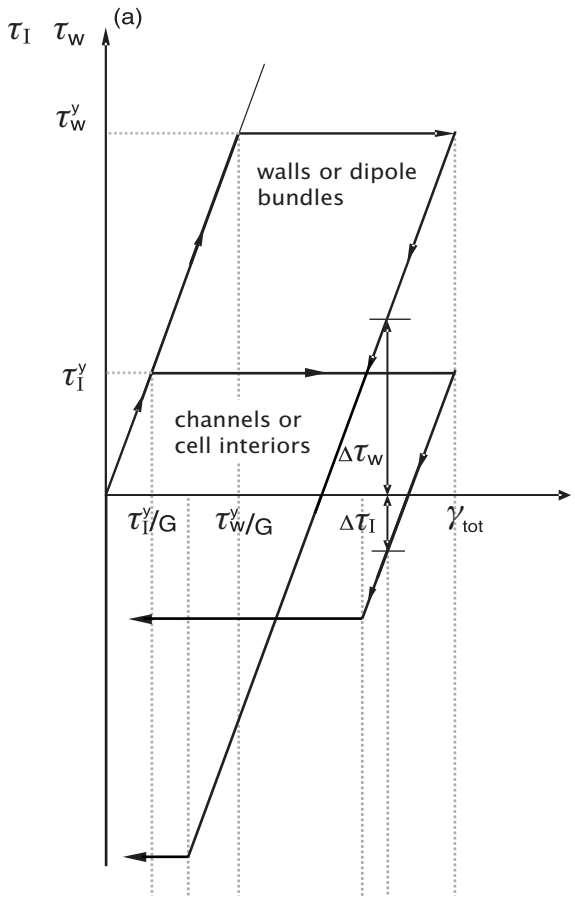


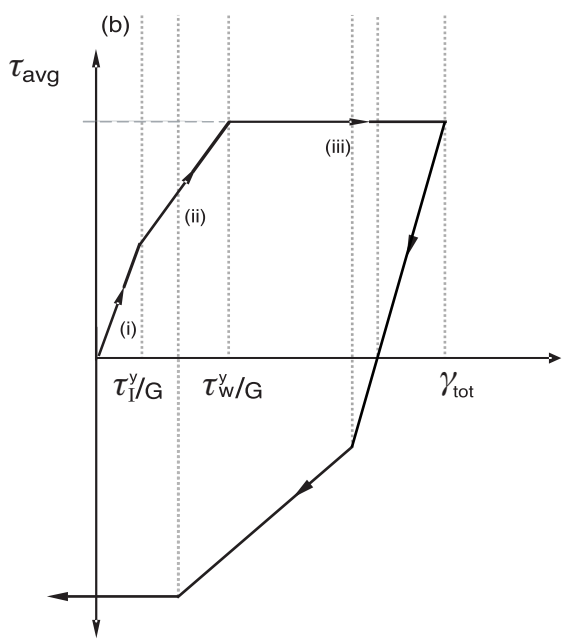

**Continuous Figure**

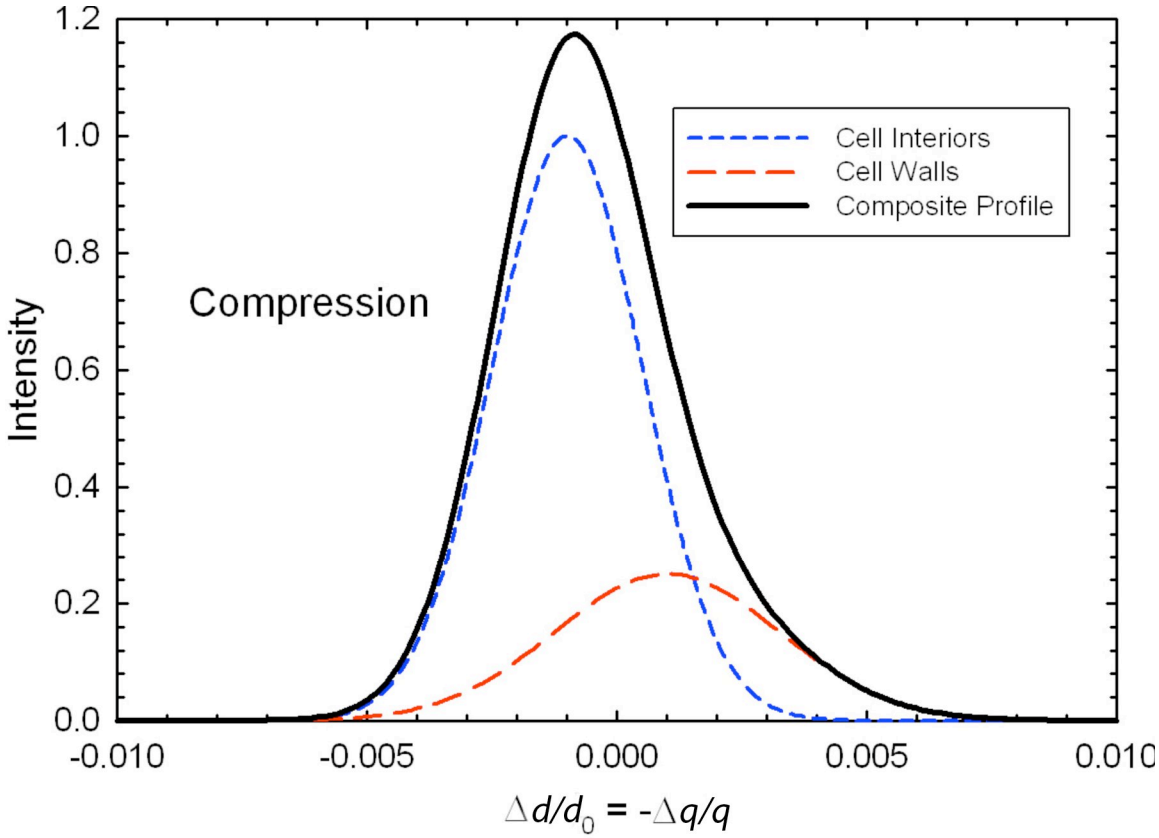


Figure 2

Colour Figure

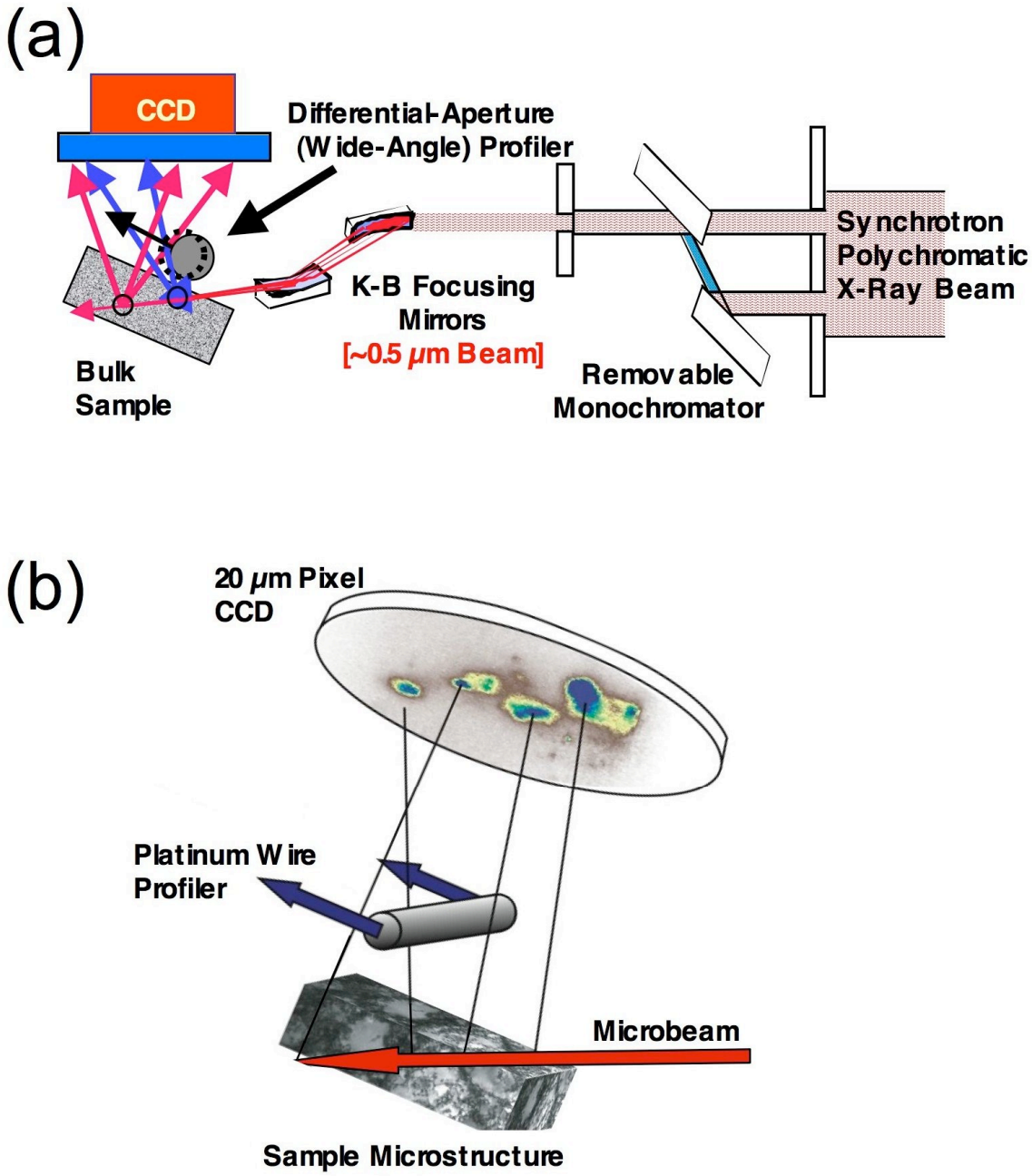


Figure 3

Continuous Figure
Click here to download high resolution image

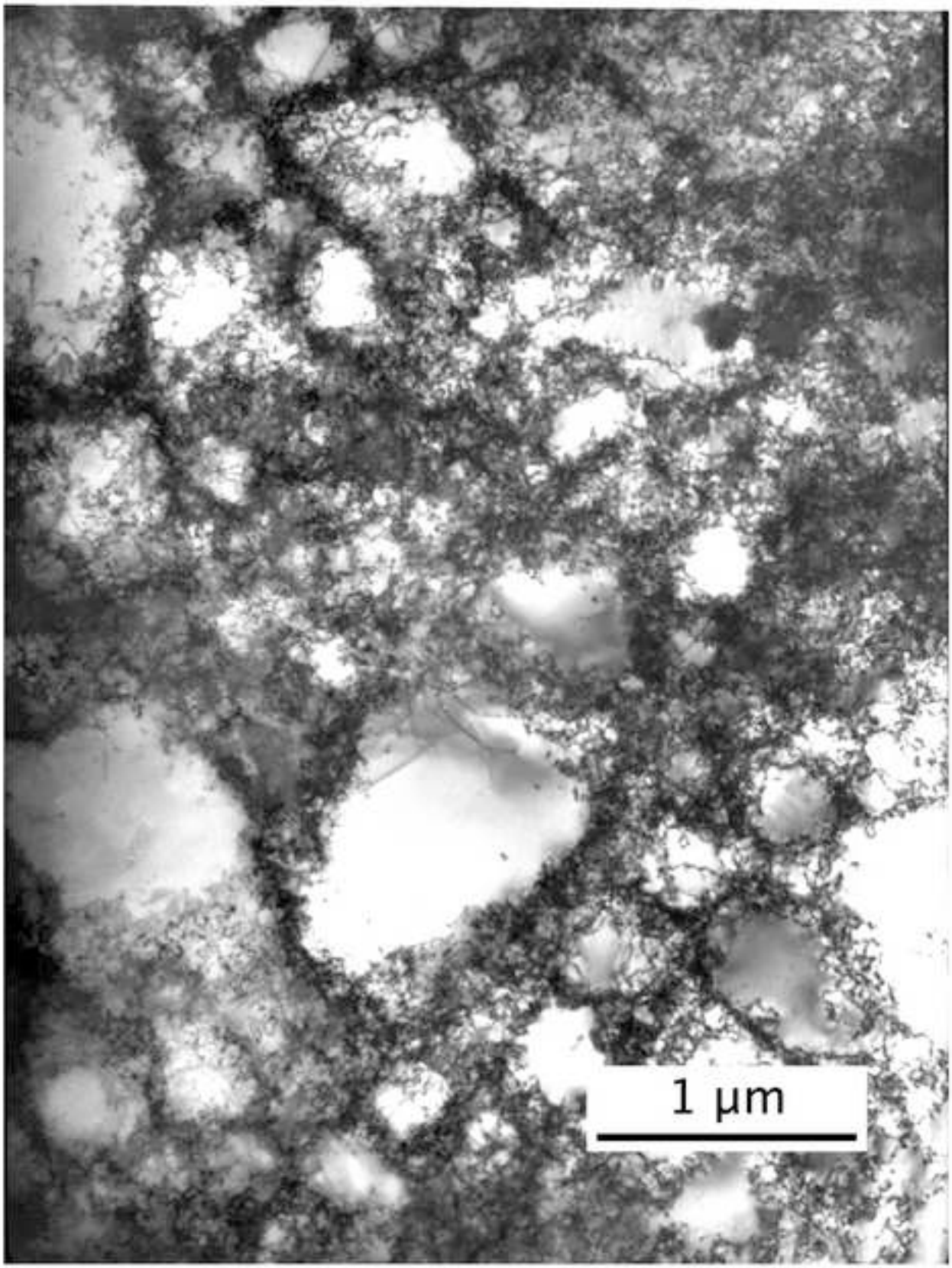


4

**Continuous Figure**

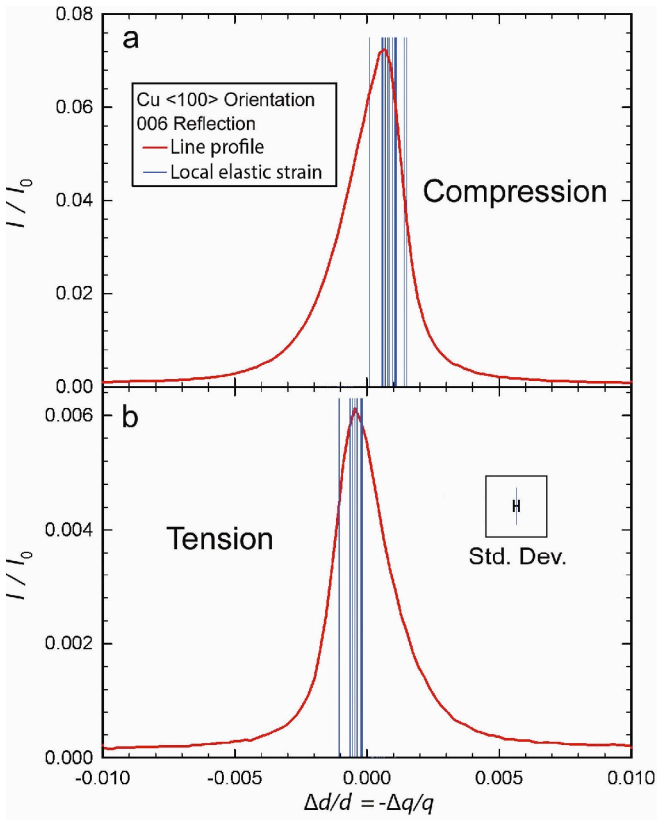


Figure 5

**Continuous Figure**

(a)

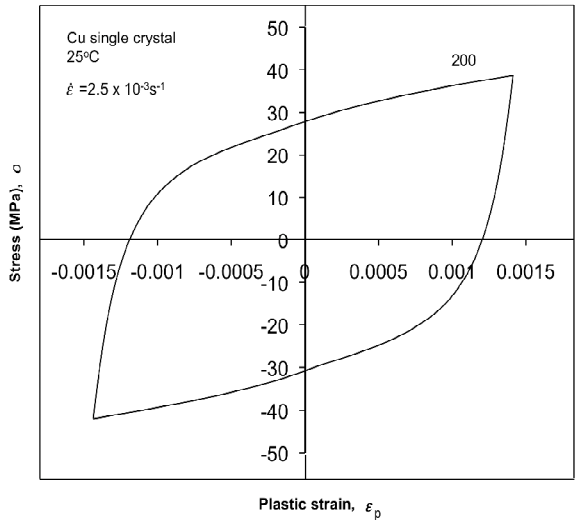


(b)

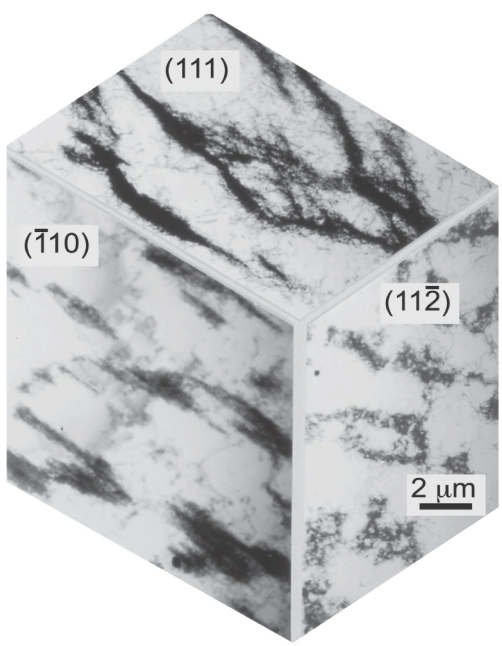

**Continuous Figure**

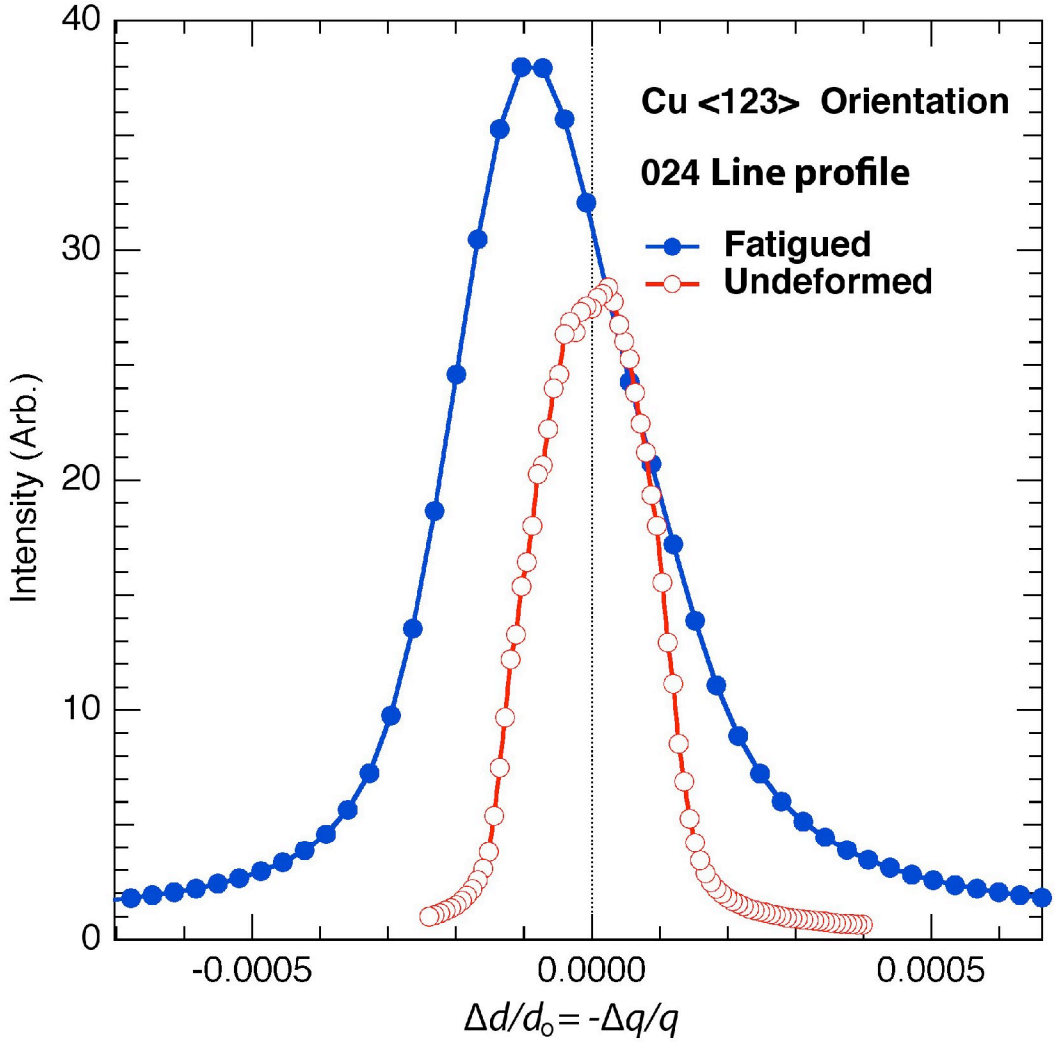


Figure 7